Journal of Alloys and Compounds 525 (2012) 44–52

Contents lists available at SciVerse ScienceDirect

Journal of Alloys and Compounds

journal homepage: www.elsevier.com/locate/jallcom

Microstructural and morphological evaluation of MCrAlY/YSZ composite produced by mechanical alloying method

M. Tahari, M. Shamanian*, M. Salehi

Department of Materials Engineering, Isfahan University of Technology, Isfahan 84156-83111, Iran

ARTICLE INFO

Article history:
Received 26 September 2011
Received in revised form 27 January 2012
Accepted 30 January 2012
Available online xxx

Keywords:
Nanocomposite
MCrAlY/YSZ
Metal matrix composite
Mechanical alloying

ABSTRACT

This paper investigates CoNiCrAlY/YSZ composite materials produced by mechanical alloying process. Various amounts of YSZ particles (0%, 5%, 10% and 15 wt.%) were mixed with CoNiCrAlY powder and milled for 12, 24 and 36 h. The structural and mechanical evolutions of the mechanically milled powders were executed using X-ray diffractometry, scanning electron microscopy, optical microscopy and micro-hardness test. It was observed that by increasing milling time, the internal lattice strain of γ-phase matrix increased while grain size of this phase decreased. Also, addition of YSZ to CoNiCrAlY decreased the rate of grain size reduction. In comparison with milled CoNiCrAlY powders, CoNiCrAlY/YSZ milled powders exhibited more spherical morphology and narrower particle size range. Moreover, the increase in milling time caused the homogenous distribution of ceramic particles in CoNiCrAlY matrix, while the increase in YSZ percent decreased the homogenous distribution of ceramic particles in CoNiCrAlY matrix. Besides, micro-hardness tests illustrated that the effect of milling on hardness is more significant than that of ceramic particles addition.

1. Introduction

MCrAlY alloys (where M is Ni, Co or Co +Ni) are one of the most famous protective coating materials applied to protect hot parts of turbines like rotary and static blades against high temperature oxidation and hot corrosion [1,2]. Eddy flows of air in gas turbines, high centrifugal force at blades and solid particles suspended in the air flow are the main failure mechanisms of protective MCrAlY coatings [2]. As there are suspended particles in the exhaust, especially when gas turbine engines serve in the dusty environment like desert region, NiCoCrAlY coating often fails due to high temperature wear [3]. Therefore, high hardness, mechanical strength and wear resistance should be provided for these protective coatings, following hot corrosion and high temperature oxidation resistance [2–4].

Therefore, some efforts have been made to increase high temperature strength and hardness of MCrAlY coatings. Strengthening metal matrix with hard particles is one of the most well-known methods for increasing high temperature strength of CoNiCrAlY. Nowadays, metal matrix composites (MMCs) are widely used at high temperatures. For instance, oxide dispersion strengthened superalloy foils prepared by advanced electron beem-physical vapor deposition (EB-PVD) technique showed excellent mechanical properties [5]. On the other hand, MMCs have been recently developed to increase strength and hardness of coatings. Cr_3C_2 and WC are conventional carbides used as reinforcement in coatings. But, due to the pyrolysis at high temperatures, they are not effective in hot stages of gas turbines (first rows) [2]. Hence, MMCs are strengthened by hard and thermally stable oxide phases. Due to particular properties at high temperatures, Al_2O_3 and Ytria Stabilized Zirconia (YSZ) are widely applied as high temperature coatings in gas turbines [6]. Thanks to the formation of oxide layer of active elements such as Hf and Y in vicinity of YSZ, this ceramic have a good wetting behavior with superalloy matrix [7]. Consequently, YSZ can be considered as a suitable reinforcement for MCrAlY because of the formation of metallic bond with metal matrix.

The high energy ball milling is a cost-effective and interesting technique for producing MMC powders [8–10]. Mechanical alloying was originally developed to produce oxide dispersion strengthened (ODS) alloys as high temperature materials by Benjamin in 1960s. The hard phases strengthen the alloy matrix by impeding the motion of dislocations. Also, the work hardening resulting from mechanical alloying leads to strengthening the ODS alloys [11]. Using this method, thermally stable MCrAlY/YSZ powders can be produced for thermal spray applications.

Another advantage of mechanical alloying is the fabrication of nanocrystalline materials [12]. Some researchers showed that the utilization of nanostructured powders as thermal spraying feedstock could greatly improve oxidation properties of MCrAlY coatings [13–15]. The improved oxidation resistance can be attributed to two main factors: (1) nanocrystalline powders will accelerate the nucleation and growth of uniform α-Al_2O_3 layer.

* Corresponding author. Tel.: +98 311 3915737; fax: +98 311 3915737.
E-mail address: shamanian@cc.iut.ac.ir (M. Shamanian).

0925-8388/$ – see front matter © 2012 Elsevier B.V. All rights reserved.
doi:10.1016/j.jallcom.2012.01.161

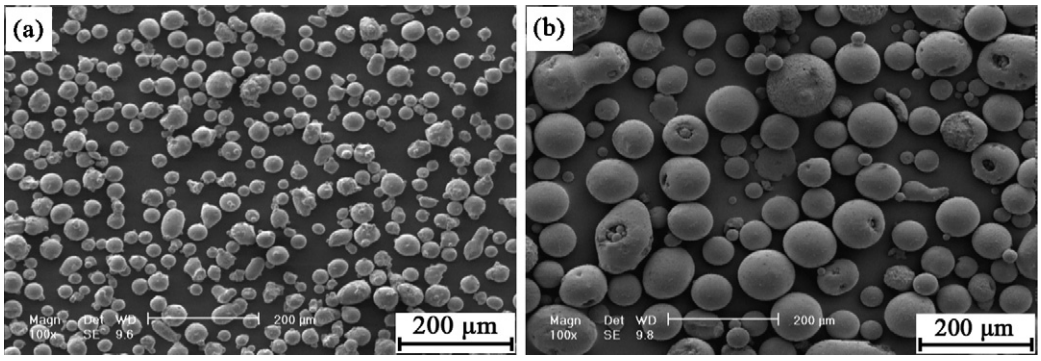

Fig. 1. Secondary electron micrographs of (a) CoNiCrAlY and (b) YSZ powders.

It could be due to the uniform distribution of aluminum in this structure. Furthermore, increasing the volume fraction of grain boundaries increases the Al diffusion rate. The grain size reduction in nanocrystalline structures also decreases the diffusion distance of Al. These factors favor the formation of a continuous α-Al_2O_3 layer as a result of Al diffusion to surface layers. (2) Improved adhesion of oxide scale to bond coat is another advantage of grain refinement reducing the oxidation rate in the bond coat [15].

In this study, CoNiCrAlY/YSZ powders were produced by mechanical milling. The microstructure, morphology and distribution of powders were also investigated.

2. Experimental procedures

The gas atomized 60.90.1 GTV was used in this study as feedstock powder. It is a commercially available spray powder CoNiCrAlY with particle size distribution ranging from 15 to 45 μm. YSZ thermal spray powder was used as reinforcement. Particle size distribution of YSZ is ranging from 20 to 120 μm. Fig. 1 shows the secondary electron micrographs of CoNiCrAlY and YSZ powders. The morphology of these powders is completely spherical. The chemical compositions of these powders are shown in Table 1.

The powders were mechanically milled in a high energy planetary ball mill at a revolution speed of 180 rpm. MM process was carried out at room temperature under argon atmosphere. The milling process was performed with the time interval of 3 h to prevent sample overheating. The stoppage time of milling was 1 h. The ball to powders weight ratio was 10:1. 10 mm diameter hardened steel balls were used for ball milling. CoNiCrAlY powders were mixed with 0%, 5%, 10% and 15 wt.% YSZ. In addition, 0.4 wt.% stearic acid was used as a process control agent (PCA) to prevent excessive cold welding of powders during milling.

For microstructural, morphological and mechanical assessments, the sampling was performed at selected time intervals. Table 2 shows numbering of these samples. X-ray diffraction (XRD) in a Philips X'PERT MPD diffractometer using filtered Cu K_α radiation (λ = 0.1542 nm) was used to estimate the crystallite size and internal lattice strain of powders using Williamson–Hall method [16–18].

$$\beta \cos\theta = \frac{k\lambda}{d} + 2A\varepsilon \sin\theta$$

where d is the average crystallite size, ε is the average internal strain, θ is Bragg diffraction angle, λ is the X-ray wavelength, β is the peak widths at half-maximum intensities (in radians), k is the Scherrer constant (0.91) and A is the coefficient dependent on the distribution of strain.

The morphological and microstructural characterization of the powder particles during MA was carried out using scanning electron microscopy (SEM) and optical microscopy (OM).

To evaluate the hardness of the composite powders and distribution of ceramics in metal matrix, a small amount of powder particles was mounted in the resin. Before indentation, the mounted powders were polished progressively using 320, 600, 1200, 2400 and 4000 sandpaper followed by 0.5 μm Al_2O_3. Vickers microhardness at the polished cross-section of powders was measured using a Vickers micro hardness tester with a load of 100 g and dwell time of 15 s. The reported hardness is the average of twenty Vickers indentation marks on each sample.

Table 1
Chemical compositions of CoNiCrAlY and YSZ powders.

Element (wt.%)	Co	Ni	Cr	Al	Y	ZrO_2	Y_2O_3
CoNiCrAlY	Bal	32	21	8	0.5	–	–
YSZ	–	–	–	–	–	92	8

Table 2
Numbering samples with different amounts YSZ and milling time.

Sample number	YSZ (wt.%)	Milling time (h)
M12	0	12
M24	0	24
M36	0	36
MY0512	5	12
MY0524	5	24
MY0536	5	36
MY1012	10	12
MY1024	10	24
MY1036	10	36
MY1512	15	12
MY1524	15	24
MY1536	15	36

3. Results and discussion

3.1. Structural characterization

Fig. 2 shows XRD patterns of as-received and milled CoNiCrAlY powders after different milling times. The phase identification studies showed that as-received CoNiCrAlY contains two main phases. Three (1 1 1), (2 0 0) and (2 2 0) sharp peaks belong to fcc-γ phase and the other peaks belong to bcc-β phase. The matrix phase, γ, consists of Co–Ni–Cr solid solution. A secondary phase, β, comprised the NiAl intermetallic [19].

It can be observed that β-phase precipitates disappear during milling process, probably due to dissolution into γ phase. It is obvious that dissolution process occurred under severe plastic deformation. Richer et al. reported similar results [19]. They suggested that crystal structure of γ-phase is more stable than that of β-phase under sever plastic deformation. Fig. 3 shows the lattice stability as a function of the average valence electrons per atom (Z) for fcc and bcc structure. It can be seen that β phase has bcc structure at equilibrium condition since this structure shows the lowest energy level for β average valence electrons per atom (Z = 6.5). According to Fig. 3, the stable crystal lattice of Co-Ni–Cr solid solution (γ phase) is fcc because the average valence electrons per atom is Z = 8.25. Fig. 3 shows that β to γ phase transformation involves an energy increase equal to Δ_1 (~7.1 kJ/mol). But the energy level of γ phase increases about Δ_2 (~21.4 kJ/mol) for fcc to bcc transformation. The severe plastic deformation during mechanical milling leads to formation of high dislocation densities in the materials. The high density of dislocation results in high average strain at atomic levels. The increases in energy and strain level are the driving force for phase transition with suitable energy and strain level. On the other hand, decreasing the energy and strain level may be caused by breaking down larger grains into finer subgrains, eventually

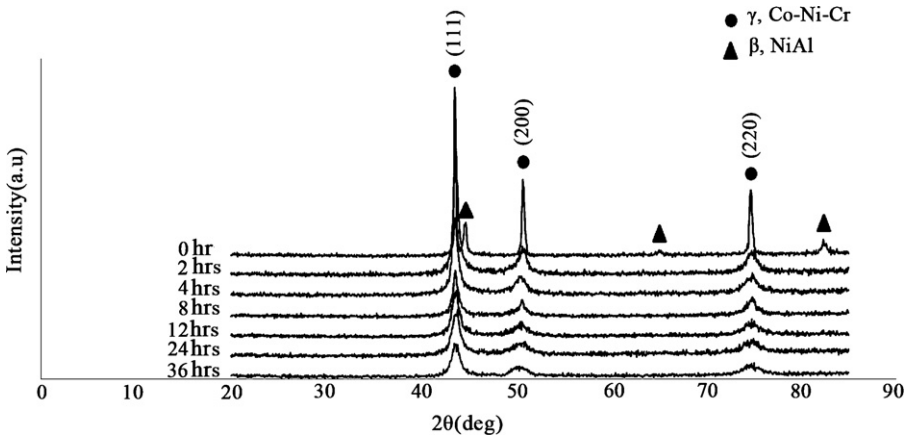

Fig. 2. XRD patterns of as-received CoNiCrAlY and CoNiCrAlY after different milling times.

resulting in grain refinement. It was showed that in atomized CoNiCrAlY powders, the β-phase precipitates are considerably finer compared with γ-phase. It was revealed that a larger portion of milling energy involves the grain refinement of γ-phase. The strain and energy level of γ-phase before phase transformation were decreased by grain refinement, while fine-grain β precipitates could not absorb high energy resulting in dissolution into γ-matrix [19]. In fact, γ-phase peaks become shorter and broader with increasing milling time. The broadening is because of grain refinement, an increase in lattice defects such as dislocations and vacancies and an increase in internal strain of crystal lattice [20–22]. In the first stage of milling, severe plastic deformation is localized into shear bands consisting of an array of dislocations with high density [23]. By increasing the milling time, at a certain strain level, a cell structure combined of dislocations is produced forming low angle grain boundaries. With increase in milling time, low angle boundaries are changed to nanocrystalline structure with random orientation. The grain size is continuously decreased until final stages at which saturated size is achieved [20,24].

The crystallite size and the internal strain of γ-phase were calculated using the Williamson–Hall equation. The results are shown in Fig. 4. At early stages of milling, with increasing milling time to 4 h, the grain size and internal strain were decreased rapidly. The crystallite size was decreased rapidly by increasing milling time from 4 to 8 h, but the growing rate of internal strain decreases. After 8 h milling, the crystallite size was decreased slowly until 24 h. Then, it reached a steady-state value of 25 nm. At the same time, the internal strain increased slowly until 24 h and then approached a constant value of 1.2%

Fig. 5(a–c) shows XRD patterns of as-received CoNiCrAlY and CoNiCrAlY samples with different YSZ contents as a function of milling time. It can be observed that in these samples, β-phase precipitates disappear due to severe plastic deformation. The grain size and internal strain of γ-phase were estimated using Williamson–Hall equation. The calculated grain size and internal strain are reported in Fig. 6(a–c). Comparing Figs. 4 and 6(a–c) shows that the addition of YSZ to CoNiCrAlY reduces the decreasing rate of grain size. The decreasing rate of grain size was further reduced with increasing YSZ. Generally, ceramic particles have two effects on milling process. Ceramic particles absorb a large portion of milling energy during their fragmentation instead of deformation of metal matrix [25–27]. On the other hand, the presence of ceramic particles in metal matrix enhances local deformation in the vicinity of the hard particles [28–30]. Here, the first mechanism seems to be dominant.

It can be observed that the internal lattice strain of γ-phase matrix was increased with increasing the amount of ceramic. Ceramic particles prevent movement and arrangement of dislocation during milling process. So, the recovery rate of dislocations was decreased with increasing hard particles. Therefore, the growing rate of internal strain was increased with the addition of YSZ.

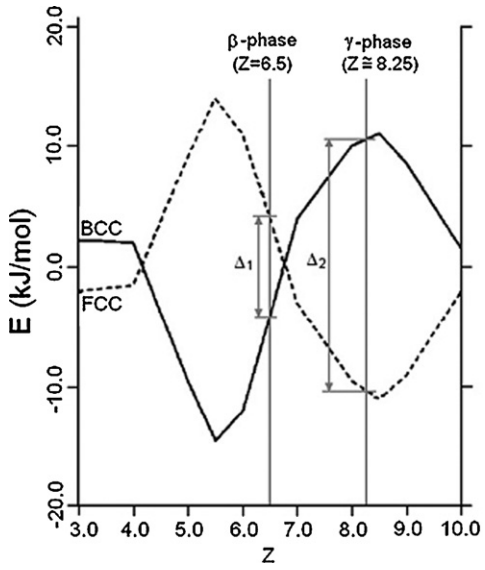

Fig. 3. Lattice stability as a function of the average number of valence electrons per atom (*Z*) for two types of crystal structure: bcc (solid curve) and fcc (dashed curve) [19].

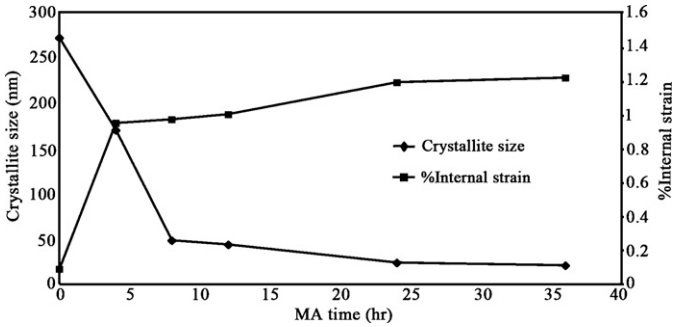

Fig. 4. Variation of crystallite size and internal strain of γ-phase in CoNiCrAlY powder with increasing milling time.

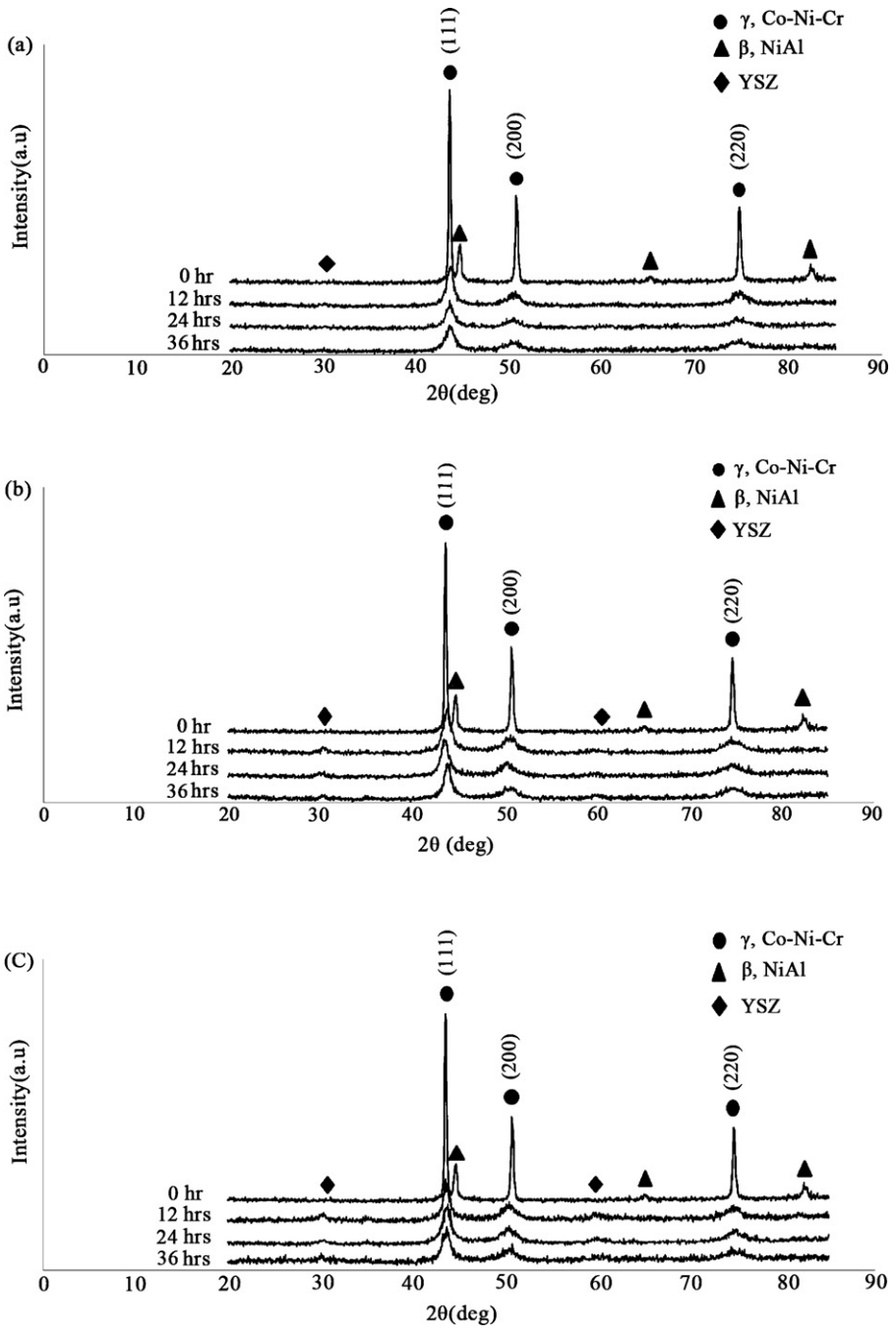

Fig. 5. XRD patterns of (a) CoNiCrAlY + 5% YSZ, (b) CoNiCrAlY + 10% YSZ and (c) CoNiCrAlY + 15% YSZ powders after different milling times.

Fogagnolo et al. showed that the presence of AlN in Al matrix increases internal strain of matrix during mechanical alloying [31].

Diagrams of ceramic content vs. grain size are shown in Fig. 7. It can be seen that by increasing YSZ at different milling times, the grain size increases. It is worth noting that the slope of these graphs decreased with increasing milling time, indicating that grain size in samples with different ceramic contents became closer to each other. Probably, more milling energy is consumed by fragment ceramic particle in the earlier stages of milling. Then, fragmented and dispersed ceramic particles in metal matrix enhanced the local deformation of matrix. So, the increase in ceramic content at long milling times facilitated deformation of matrix. Therefore, the differences in grain size are decreased.

3.2. Morphological evaluations

Fig. 8(a–l) shows secondary electron micrograph of MCrAlY/YSZ powders at different milling times. The collisions among the powders, balls and the vial walls result in severe plastic deformation, cold welding and fragmentation of powder particles in different stages of mechanical milling. During initial stages, plastic deformation and cold welding are the dominant phenomena. Then, work hardening and fracture occur [32–34]. Finally, there will be a balance between welding and fracturing of powders resulting in the formation of particles with approximately equiaxed morphology. This stage is known to be steady state conditions because particle size and distribution size of particles are in equilibrated conditions [33,35].

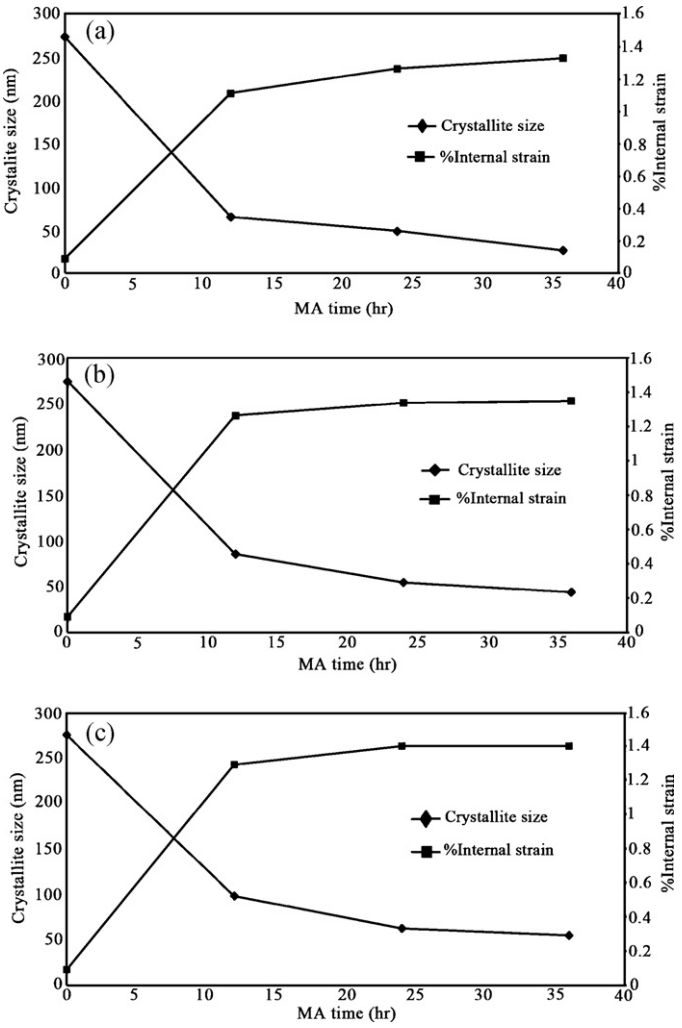

Fig. 6. Variations of crystallite size and internal strain of γ-phase in (a) CoNiCrAlY + 5% YSZ, (b) CoNiCrAlY + 10% YSZ and (c) CoNiCrAlY + 15% YSZ powders with increasing milling time.

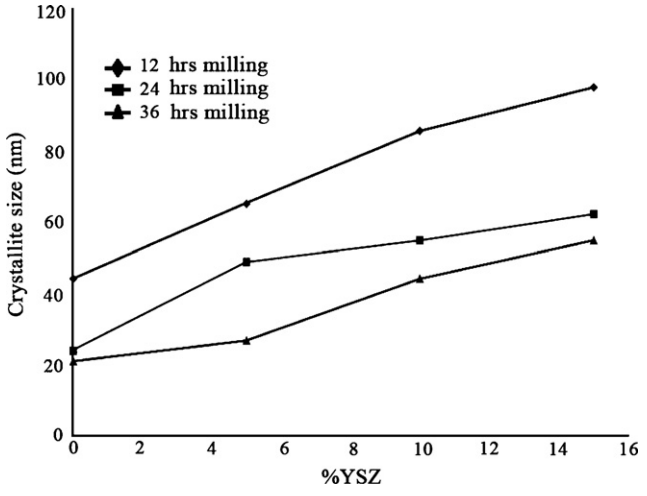

Fig. 7. The effect of YSZ percent on crystallite size of γ-phase of powders at 12, 24 and 36 h milling time.

Fig. 8(a) shows that CoNiCrAlY particles were enlarged due to cold welding and their morphology seems to be flake-like due to severe plastic deformation. This shows that cold welding is the predominant phenomenon until 12 h milling. It can be seen that CoNiCrAlY powders became finer and somewhat spherical after 24 h milling (Fig. 8(b)). It seems that cold welding and fragmentation of work hardened particles have occurred simultaneously. However, the cold welding is still the dominant phenomenon. Fig. 8(c) shows that CoNiCrAlY powder is fine and somewhat spherical after 36 h milling. Sachan et al. reported a similar behavior during the ball milling process [36]. But, it is clear that the steady state conditions are not reached yet because the powder morphology is not spherical completely and particle distribution is not uniform.

Fig. 8(d–f) shows the morphology of CoNiCrAlY + 5% YSZ powders after 12, 24 and 36 h of milling. It can be observed that the addition of YSZ to CoNiCrAlY prevented the formation of flake-like morphology and large particles at initial stages of milling (Fig. 8(d)). The powder presents a compact and rounded but not flattened morphology. Powder particles with a high deformation capability usually show such a morphology at the initial stage of mechanical milling, where cold welding is the main mechanism in this stage [28]. It can be seen that with increasing the milling time, more coarse particles are formed (Fig. 8(e)). In addition, the amount of fine particles has been increased too. Probably, continued cold welding after 12 h milling causes the formation of large particles. Then, fracturing mechanism is started and large particles are fragmented to finer particles. With increasing the milling time, fracturing became the predominant phenomenon so that fragmentation of large particles increases. It can be observed that after 36 h milling, most of the particles have a similar size and distribution (Fig. 8(f)). It can be seen after 36 h milling, MA process has reached the steady state condition.

Comparison of Fig. 8(d and e) with (g and h) shows that increasing the ceramic content delays the formation of large particles formed in powder containing 10% YSZ. It was previously demonstrated that increasing the ceramic content decreases plastic deformation rate at the initial stages of mechanical milling. Hence, the presence of large particles of YSZ and the decrease of plastic deformation delay cold welding phenomenon. On the other hand, the presence of ceramic particles enhanced brittleness of powders containing 10% YSZ in comparison with 5% YSZ powder. So, the final particles of 10% YSZ are finer than those of 5% YSZ powders after 36 h milling (Fig. 8(i)) [34]. Fig. 8(j–l) confirms the above discussions. But, it can be observed that increasing the ceramic content decreases the powder particle size [37]. The increase in fracture rate of composite powder along with the increase in the amount YSZ results in the formation of equiaxed and fine composite particles in comparison with unreinforced powders. Other researchers also reported that ceramic particles decrease the milling time needed for reaching steady state condition [34]. Additionally, the presence of YSZ particles resulted in the formation close particle-size distribution of particles.

To assess the predominant mechanisms in different stages of mechanical milling, the secondary micrograph of fracture surface of powders was investigated. Fig. 9 shows that in the initial steps of mechanical milling, fracture surfaces are completely ductile and plastic deformation is dominant. As milling time increased, ductile fracture was transformed to brittle fracture. These demonstrate that increasing milling time promotes brittleness of powders. On the other hand, Fig. 9 shows that with increasing the amount of YSZ in composite powders, the ductile to brittle fracture transformation has been delayed. It can be observed that although brittleness of 15% YSZ powder is lower than that of 5% YSZ powder, it shows a finer particle. The presence of YSZ particles in metal matrix has facilitated crack growth and fracture in powder particles.

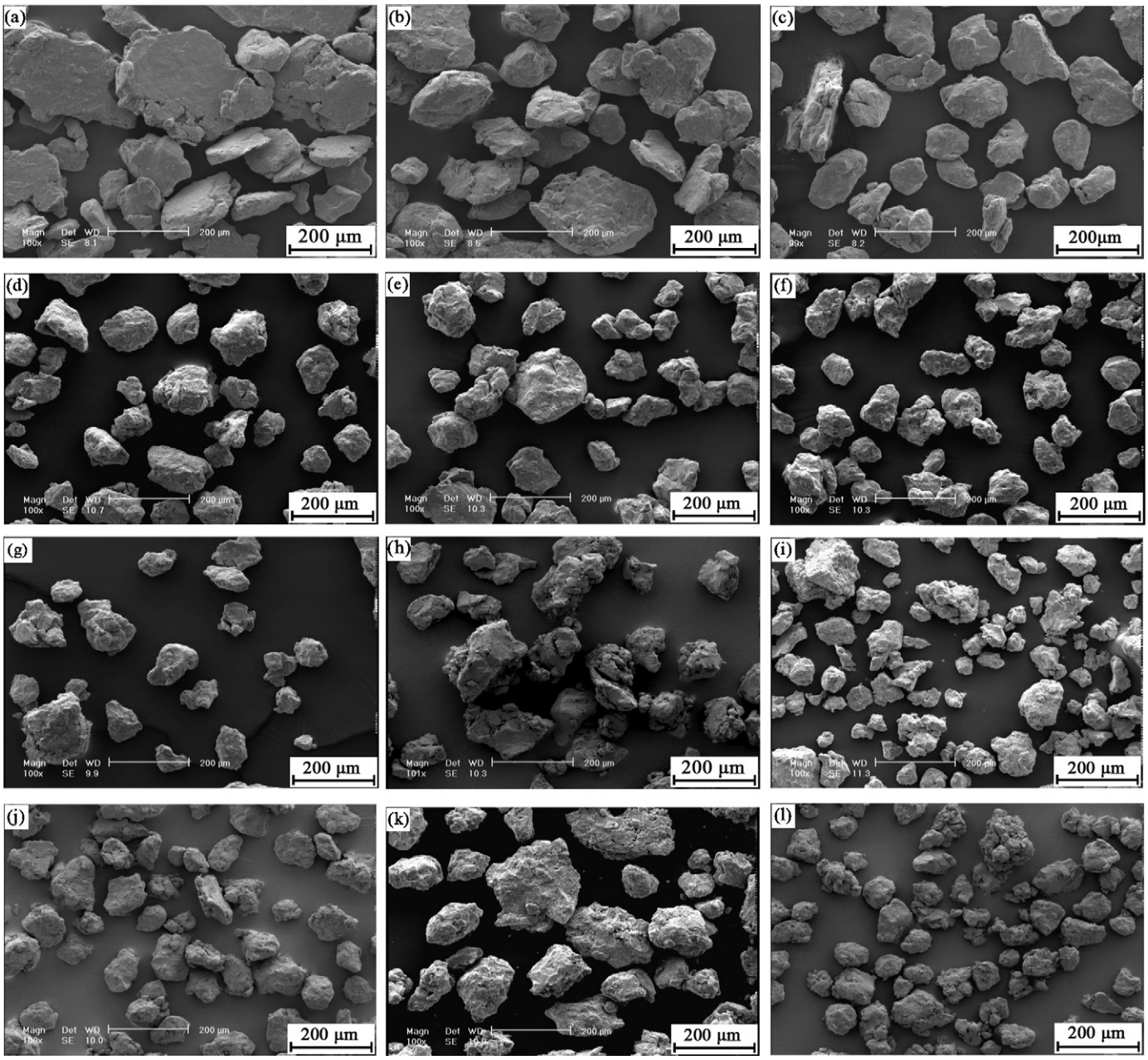

Fig. 8. Secondary electron micrographs of variations of particle morphology of (a) M12, (b) M24, (c) M36, (d) MY0512, (e) MY0524, (f) MY0536, (g) MY1012, (h) MY1024, (i) MY1036, (j) MY1512, (k) MY1524, and (l) MY1536 powders.

3.3. Microstructure evaluation

The presence of hard particles mixed with CoNiCrAlY changed the milling classification to a ductile/brittle system. In the first stage of milling, the predominant mechanism is the fragmentation of hard particles and plastic deformation of ductile particles. Then, due to collisions, hard particles are embedded in cold welded ductile particles. As a result, fine reinforcement particles will be confined in the interfacial boundaries of the agglomerated metal particles causing the formation of a real composite particle [18,29].

To evaluate the distribution and size of YSZ particles in CoNiCrAlY matrix, back scattered SEM and optical micrographs were used. Fig. 10 shows the distribution of YSZ in CoNiCrAlY matrix in the powders containing 15% YSZ. Since the average atomic number of YSZ is greater than that of CoNiCrAlY, these particles seem brighter than matrix in back scattered micrographs. It can be observed that in the first stage of milling (after 12 h), YSZ particles are visible. But, with increasing milling time, YSZ particles are invisible at 1000× magnification because the size of YSZ powders is decreased. Zhao et al. showed that increase in milling time resulted in the fragmentation of hard particles due to the impacts of balls [38]. On the other hand, the increase in milling time caused the homogenous distribution of reinforcements in the matrix [28,38]. Fig. 11 shows distribution of hard particles in CoNiCrAlY matrix in optical micrographs. It can be seen that YSZ particles have been homogeneously dispersed in the alloy and their size is reduced with increasing milling time. As YSZ content was increased, the distribution became inhomogeneous and the final powder size is raised. The higher the amount of ceramic content, the higher the energy needed for structural refinement.

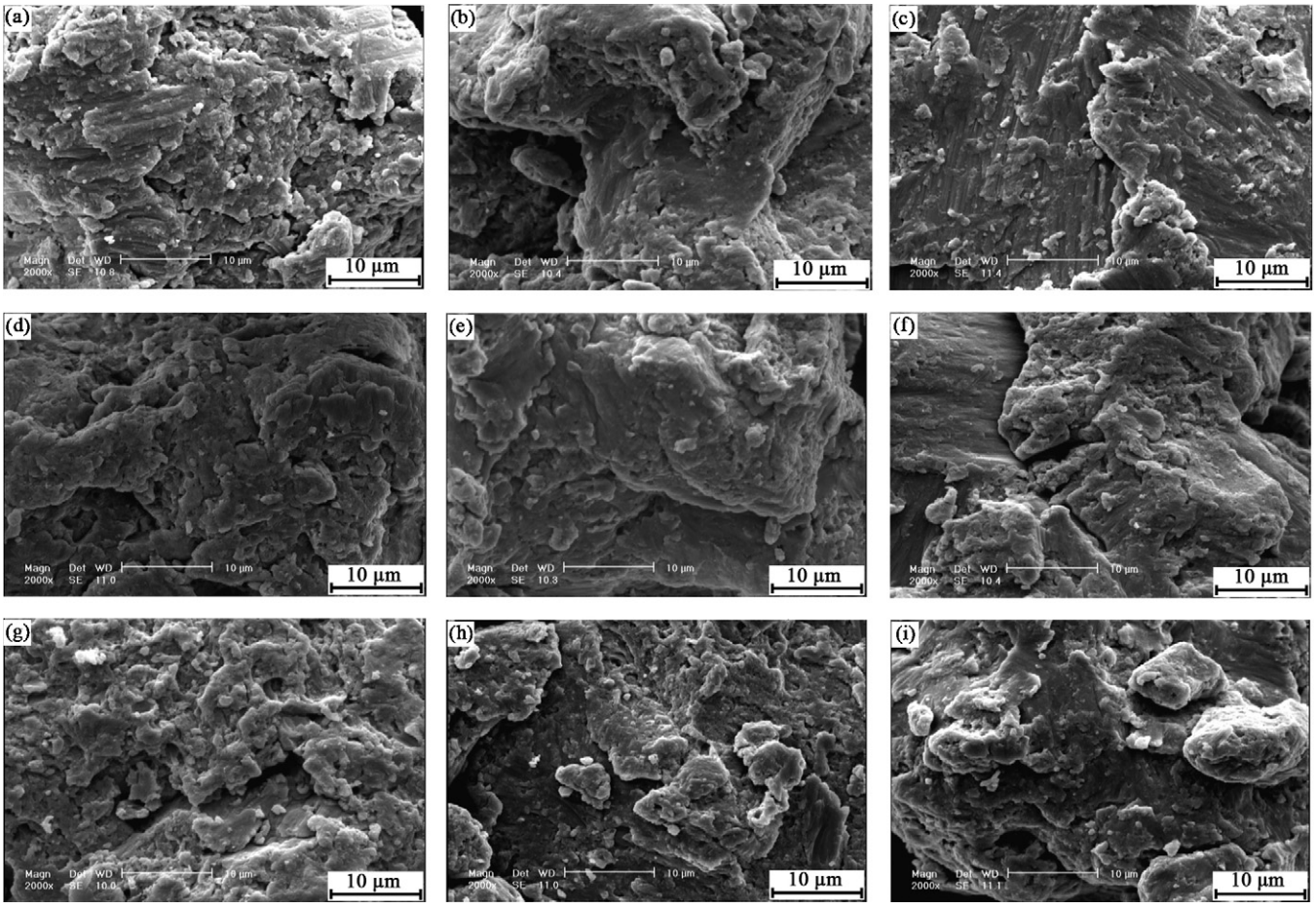

Fig. 9. Secondary micrograph of fracture surface of (a) MY0512, (b) MY0524, (c) MY0536, (d) MY1012, (e) MY1024, (f) MY1036, (g) MY1512, (h) MY1524, and (i) MY1536 powders.

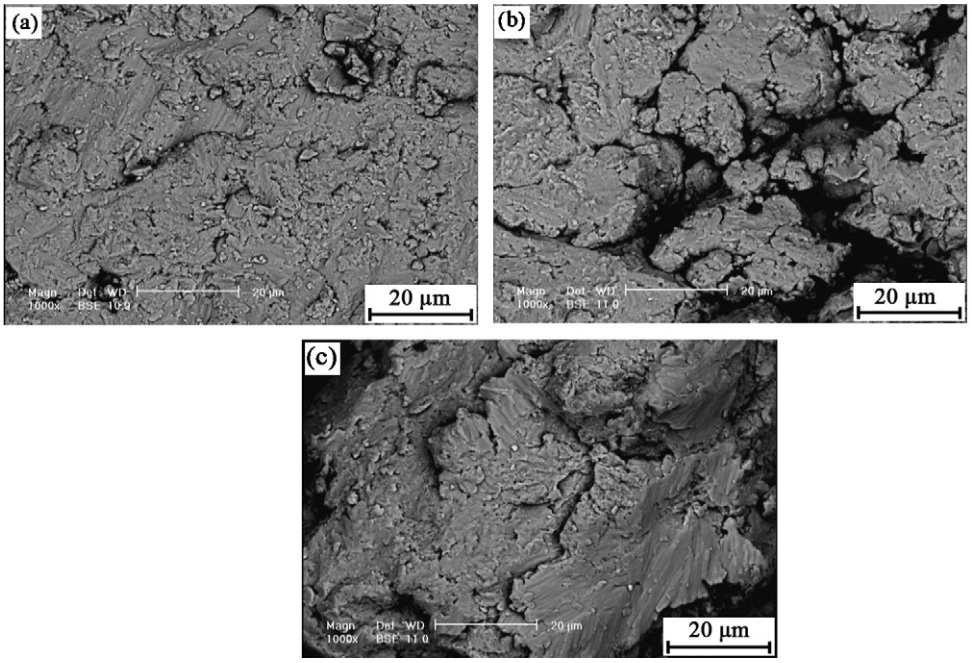

Fig. 10. Back scattered micrograph of distribution and size of YSZ particles in CoNiCrAlY matrix in (a) MY1512, (b) MY1524 and (c) MY1536.

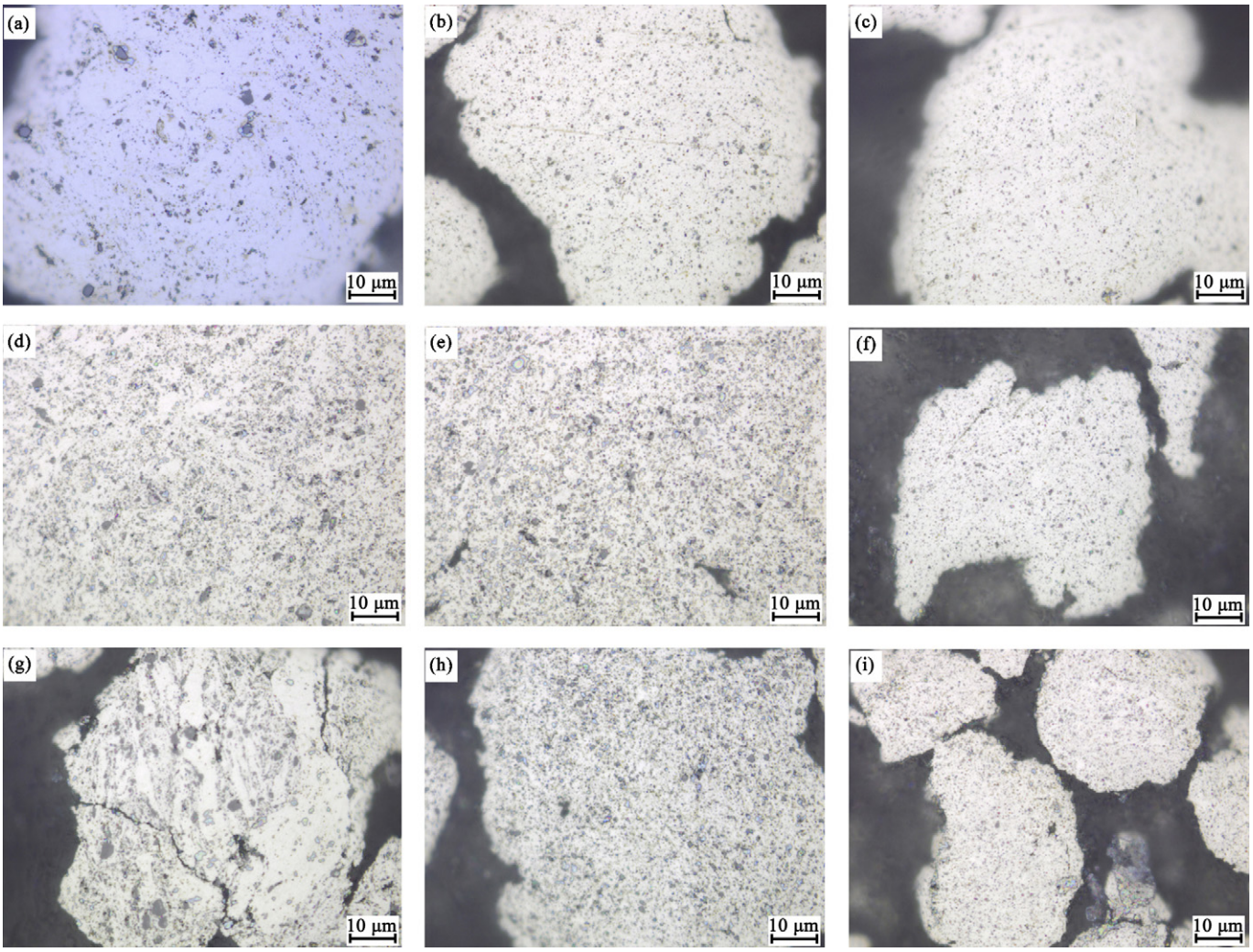

Fig. 11. Distribution of hard particles into CoNiCrAlY matrix in (a) MY0512, (b) MY0524, (c) MY0536, (d) MY1012, (e) MY1024, (f) MY1036, (g) MY1512, (h) MY1524, and (i) MY1536 powders.

3.4. Microhardness measurements

The most important hardening mechanisms of metals and alloys are deformation, grain refinement and solid dispersion [29,39]. One of the well-known methods for producing hard materials through these mechanisms is mechanical alloying.

Mechanical alloying involves a high degree of deformation which can reduce the grain size to nanometer level and produce an extremely fine distribution of hard particles in a metal matrix [29]. According to Orowan mechanism, hard particles reinforcements act as a barrier to the dislocation movement within the matrix and exhibit greater resistance to indentation of the hardness tester [40]. Unlike as-received CoNiCrAlY powders, milled powders have a high density of dislocations due to severe plastic deformation. Recovery of dislocations results in the refinement of microstructure during milling process. Therefore, milled powders exhibit higher hardness in comparison with as-received powders. The hardness of milled and as-received powders is presented in Fig. 12. Two factors affect the hardness of the composite powders. One is the effect of fine dispersion of reinforcement and the other is the effect of mechanical alloying process and severe plastic deformation on the metal matrix. These results showed that the effect of fine dispersion of reinforcement on the hardness is lower than that of mechanical milling process. The hardness of composite powders and unreinforced powders under the same mechanical milling conditions seems to be similar. But, the hardness of mechanically milled unreinforced matrix is twice higher than that of as-received powders. Fogagnolo et al. reported similar results for Al/AlN composite powder [29]. It can be observed that at

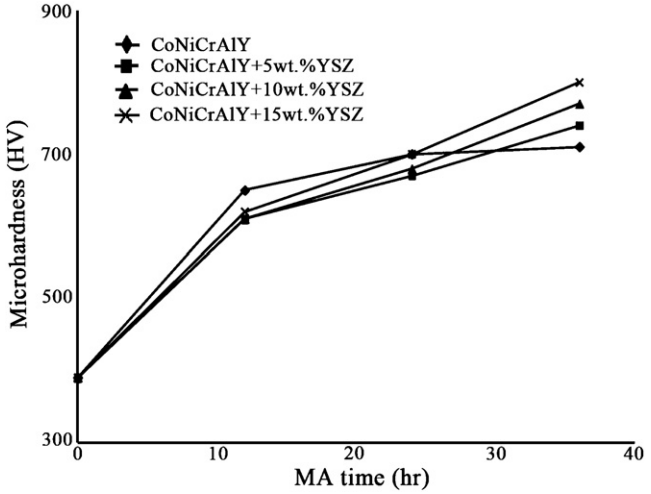

Fig. 12. Hardness of the milled powders with respect to the mechanical milling time.

initial times of milling (24 h), unreinforced powders are harder than composite powders, but with increasing milling time, composite powders became harder. It was previously said that large particles of YSZ decreased plastic deformation tendency of composite powders. So, these powders exhibit lower hardness at initial stages. Unlike unreinforced powders, increasing milling time increases hardness of composite powders. It can be due to the homogeneous distribution of hard particles, increasing internal strains, inhibited recovery of dislocations and the decrease in grain size.

4. Conclusions

CoNiCrAlY/YSZ composite powders were synthesized using MA technique. The following conclusions can be drawn:

- The grain size of CoNiCrAlY decreased with increasing the milling time. The addition of YSZ delayed the decrease in grain size of matrix.
- Increasing the milling time and YSZ percent resulted in the spherical morphology and homogenous distribution of powders. The addition of YSZ also delayed cold welding phenomenon.
- At initial stage of milling, CoNiCrAlY powder showed the greatest hardness but with increasing the milling time powders containing 15% YSZ, it showed the maximum hardness.

References

[1] T. Liang, H. Guo, H. Peng, S. Gonga, J. Alloys Compd. 509 (2011) 8542–8548.
[2] K. Bobzin, T. Schla fer, K. Richardt, M. Bruhl, J. Therm. Spray Technol. 17 (2008) 853–857.
[3] W.H. Yu, Z.D. Wen, W.M. Di, S.G. Fang, M. Hong, S.Yu. Li, Trans. Nonferrous Met. Soc., China 21 (2011) 1322–1328.
[4] Y. Xie, M. Wang, J. Alloys Compd. 484 (2009) 21–24.
[5] H. Peng, H. Guo, J. He, S. Gong, J. Alloys Compd. 502 (2010) 411–416.
[6] A. Keyvani, M. Saremi, M. Heydarzadeh Sohi, J. Alloys Compd. 509 (2011) 8370–8377.
[7] F. Valenza, M.L. Muolo, A. Passerone, J. Mater. Sci. 45 (2010) 2071–2079.
[8] M. Khakbiz, F. Akhlaghi, J. Alloys Compd. 479 (2009) 334–341.
[9] A. Vyasa, K.P. Raob, Y.V.R.K. Prasadb, J. Alloys Compd. 475 (2009) 252–260.
[10] H. Ahamed, V. Senthilkumar, J. Alloys Compd. 505 (2010) 772–778.
[11] C.C. Koch, Mater. Sci. Eng. A 244 (1988) 39–48.
[12] M. Krasnowski, T. Kulik, J. Alloys Compd. 448 (2008) 227–233.
[13] F. Tang, L. Ajdelsztajn, G.E. Kim, V. Provenzano, J.M. Schoenung, Fundamental Science of Energy 004, Berkeley, California, 2002.
[14] D. Mercier, B.D. Gauntt, M. Brochu, Surf. Coat. Technol. 205 (2011) 4162–4168.
[15] D. Mercier, C. Kaplin, G. Goodall, G. Kimb, M. Brochu, Surf. Coat. Technol. 505 (2010) 2546–2553.
[16] A.R. Abbasi, M. Shamanian, J. Alloys Compd. 508 (2010) 152–157.
[17] M. Azimi, G.H. Akbari, J. Alloys Compd. 509 (2011) 27–32.
[18] H. Abdoli, E. Salahi, H. Farnoush, K. Pourazrang, J. Alloys Compd. 461 (2008) 166–172.
[19] P. Richer, A. Zuniga, M. Yandouzi, B. Jodoin, Surf. Coat. Technol. 203 (2008) 364–371.
[20] N. Parvina, R. Assadifarda, P. Safarzadeha, S. Sheibani, P. Marashi, Mater. Sci. Eng. A 492 (2008) 134–140.
[21] A. Genc, M.L. Ovecoglu, J. Alloys Compd. 508 (2010) 162–171.
[22] H. Zuhailawati, Y. Mahani, J. Alloys Compd. 476 (2009) 142–146.
[23] J. Lee, F. Zhou, K.H. Chung, N.J. Kim, E.J. Lavernia, Metall. Mater. Trans. A 32A (2001) 3109–3115.
[24] F. Karimzadeh, M.H. Enayati, M. Tavoosi, Mater. Sci. Eng. A 486 (2008) 45–48.
[25] H. Kaftelen, M.L. Ovecoglu, H. Henein, H. Cimenoglu, Mater. Sci. Eng. A 527 (2010) 5930–5938.
[26] A. Bhaduri, V. Gopinathan, P. Ramakrishnan, A.P. Miodownik, Metall. Mater. Trans. A 27A (1996) 3718–3726.
[27] S. Kumaran, T. Sasikumar, R. Arockiakumar, T. Srinivasa Rao, Powder Technol. 185 (2008) 124–130.
[28] E.M. Ruiz-Navas, J.B. Fogagnolo, F. Velasco, J.M. Ruiz-Prieto, L. Froyen, Composites A 37A (2006) 2114–2120.
[29] J.B. Fogagnolo, F. Velasco, M.H. Rober, J.M. Torralba, Mater. Sci. Eng. A 342 (2003) 131–143.
[30] S. Sivasankaran, K. Sivaprasadb, R. Narayanasamya, P.V. Satyanarayana, Mater. Charact. 62 (2011) 661–672.
[31] J.B. Fogagnolo, M.H. Robert, J.M. Torralba, Mater. Sci. Eng. A 426 (2006) 85–94.
[32] S. Scudino, M. Sakaliyska, K.B. Surreddi, J. Eckert, J. Alloys Compd. 483 (2009) 2–7.
[33] S.M. Zebarjad, S.A. Sajjadi, Mater. Des. 27 (2006) 684–688.
[34] S. Sivasankaran, K. Sivaprasad, R. Narayanasamy, V.K. Iyer, Powder Technol. 201 (2010) 70–82.
[35] N. Parvina, R. Assadifarda, P. Safarzadeha, S. Sheibani, P. Marashi, Mater. Sci. Eng. A 492 (2008) 1340–2140.
[36] R. Sachan, J.W. Park, J. Alloys Compd. 485 (2009) 724–729.
[37] S.S. Razavi-Tousi, R. Yazdani-Radb, S.A. Manafi, Mater. Sci. Eng. A 528 (2011) 1105–1110.
[38] N. Zhao, P. Nash, X. Yang, J. Mater. Process. Technol. 170 (2005) 586–592.
[39] Z. Sadeghiana, B. Lotfia, M.H. Enayati, P. Beissc, J. Alloys Compd. 509 (2011) 7758–7763.
[40] M. Sameezadeh, M. Emamy, H. Farhangi, Mater. Des. 32 (2011) 2157–2164.